DOE/BC/15311-9
(OSTI ID: 793652)

FOSSIL ENERGY

EXPERIMENTAL AND ANALYTICAL STUDY OF MULTIDIMENSIONAL IMBIBITION IN FRACTURED POROUS MEDIA

SUPRI TR-129
October 2001

By
E.R. Rangel-German
A.R. Kovscek

Date Published: May 2002

Work Performed Under Contract No. DE-FC26-00BC15311

Stanford University
Stanford, California

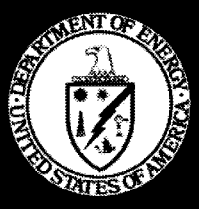

National Energy Technology Laboratory
National Petroleum Technology Office
U.S. DEPARTMENT OF ENERGY
Tulsa, Oklahoma

DOE/BC/15311-9
Distribution Category UC-122

Experimental and Analytical Study of Multidimensional Imbibition in Fractured Porous Media

By
E.R. Rangel-German
A.R. Kovscek

May 2002

Work Performed Under DE-FC26-00BC15311

Prepared for
U.S. Department of Energy
Assistant Secretary for Fossil Energy

Tom Reid, Project Manager
National Petroleum Technology Office
P.O. Box 3628
Tulsa, OK 74101

Prepared by
Stanford University
Department of Petroleum Engineering
Green Earth Sciences Bldg., Room 080B
367 Panama Street
Stanford, CA 94305-2220

TABLE OF CONTENTS

LIST OF TABLES

LIST OF FIGURES

Acknowledgement

This work was prepared with the support of U.S. Department of Energy, under Award No. DE-FC26-00BC15311. However, any opinions, findings, conclusions, or recommendations expressed herein are those of the authors and do not necessarily reflect the views of the DOE. The support of the Stanford University Petroleum Research Institute (SUPRI-A) Industrial Affiliates and Consejo Nacional de Ciencia y Tencnología (CONACyT), México is gratefully acknowledged.

Abstract

Capillary imbibition is an important mechanism during water injection and aquifer influx in fractured porous media. Better understanding of matrix-fracture interaction and imbibition in general is needed to model effectively these processes. Using an X-ray computerized tomography (CT) scanner, and a novel, CT-compatible core holder, we performed a series of experiments to study air and oil expulsion from rock samples by capillary imbibition of water in a three-dimensional geometry. The air-water system is useful in that a relatively large number of experiments can be conducted to delineate physical processes. Different injection rates and fracture apertures were utilized. Two different fracture flow regimes were identified. The "filling-fracture" regime shows a plane source that grows in length due to relatively slow water flow through fractures. In the second, "instantly-filled fracture" regime, the time to fill the fracture is much less than the imbibition time. Here, imbibition performance scales as the square root of time. In the former regime, the mass of water imbibed scales linearly with time.

A new analytical model is proposed for filling fractures incorporating implicit matrix/fracture coupling. Good agreement is found between experiments and calculation. This analytic coupling was obtained by means of solving the saturation diffusion equation with appropriate initial and boundary conditions. The solution provides the location of the wetting phase front in the fracture and the saturation distribution in the matrix. The solution is analogous to that obtained by Marx and Langenheim (1959) for the areal extent of an equivalent heated zone in thermal recovery methods. Analogous terms among flow and heat transfer in porous media were found and are also presented.

1. Introduction

Fractured petroleum reservoirs represent over 20% of the world's oil reserves (Saidi, 1983). Examples of prolific hydrocarbon reservoirs include the Monterey Shales in California, the West Texas Carbonates, the North Sea Chalks, and the Asmari Limestones in Iran. These fields (gas, oil, or both) generally have active aquifers associated with them, and most will eventually go through a process of secondary hydrocarbon recovery by waterflooding. Fractured reservoirs are also found in the geothermal industry, where produced water is reinjected to maintain reservoir pressure and/or avoid environmental problems associated with water disposal. Fractured porous media are usually divided into matrix and fracture systems. The matrix system contains most of the fluid storage, but fluid movement is slow. Fractures contain little fluid relative to the matrix, but fluids flow more easily. Flow equations are written such that recovery is dominated by the transfer of fluid from the matrix to the high conductivity fractures. In the dual-porosity formulation, fractures are entirely responsible for flow between blocks and flow to wells, while the dual permeability formulation allows some fluid movement between matrix blocks (Kazemi and Gilman, 1993). The rate of mass transfer between the rock matrix and fractures is significant and calculation of this rate depends on matrix-fracture transfer functions incorporating the shape factor.

Intuitively, we expect injected water to flow primarily through low-flow-resistance fractures rather than the high-flow resistance matrix when capillary imbibition forces are weak. Unless imbibition forces are strong enough to pull water into the matrix and expel nonwetting fluid, there will be no mass transfer between matrix and fractures. Thus, capillary forces must be relatively strong if both water injection and oil recovery in fractured systems are to be successful. Without imbibition, water will propagate through the fracture network and not enter the matrix. The injection will fail and oil recovery will be low (Akin *et al.*, 2000). Water propagation (and multiphase flow) in fractured reservoirs depends upon, at least, the combined, effects of hydraulic connectivity and wettability of fractures, rock matrix permeability and porosity, matrix-block size, capillary pressure, and the interfacial tension between the resident and the imbibing phase.

Whereas most experimental studies have focused upon single factors important to imbibition, the purpose of this study is to investigate the rate of fracture to matrix transfer and the pattern of wetting fluid imbibition as a function of the rate of water propagation in a fracture. Porous media used here are water wet. We describe a laboratory flow apparatus built to image quantitatively fluid saturation distribution in horizontal single-fracture systems. Fracture aperture and flow rate are varied. Porosity and saturation calculations along the cores were made utilizing an X-ray computerized tomography (CT) scanner. We concentrate primarily upon the water-air system because of the relative speed with which such experiments can be conducted. A range of parameters can be examined and imbibition physics probed fully. Additionally, the shape factor necessary for dual-continuum approaches, such as dual porosity, is independent of viscosity and can be obtained from the results of water-air experiments. Experiments with oil and water are also conducted to verify qualitative agreement between air-water and oil-water systems. After description of the experiments, an analytical, hydraulic-diffusivity-based method with implicit

fracture/matrix coupling is developed to calculate the mass of water imbibed. It offers a simple routine for obtaining iso-saturation curves and the extent of imbibition. The method is validated by matching the experimental data. Before proceeding to the experimental apparatus and results, our new work is put into context by reviewing literature on capillary imbibition.

2. Related Literature

Most experimental studies of flow in fractured rocks have focused upon individual components of the overall problem, such as single and multiphase flow in fractures bounded by impermeable rock or imbibition in single matrix blocks of variable size. Several studies have focused on understanding properties of fractured porous media such as capillary pressure, continuity between adjacent matrix blocks, fracture relative permeabilities, and cocurrent or counter-current imbibition (Kazemi *et al.*, 1989; Mattax and Kyte, 1962; Hughes, 1995; Cil *et al.*, 1998; Rangel-German, 1998; Rangel-German *et al.*, 1999). Other studies have attempted to delineate differences between cocurrent and countercurrent imbibition (Pooladi-Darvish and Firoozabadi, 2000).

Regarding flow in isolated fractures, Romm (1966) presented two-phase flow experiments between smooth, vertical, parallel plates. He found that fracture relative permeabilities are equal to the phase saturation. He stated that these results could not be applied to flow in fractured media where a system of interconnected fractures is present. Jones *et al.*, 1990) studied-single phase flow through rough-walled fractures, and found that for wide fractures, Whitherspoon *et al.*'s (1980) cubic law equation can be used to calculate absolute permeability and to characterize single-phase flow. Persoff and Pruess (1995) dealt with rough-walled fractures using epoxy replicas. They obtained the best possible matches for an isolated fracture. Their results suggest that fracture relative permeability should not be considered as a straight line with a value equal to phase saturation. On the other hand, Pan and Wong (1996) showed that straight-line fracture relative permeabilities can be used, but they also stated that the values are not necessarily equal to the phase saturation. These observations were verified by Rangel-German *et al.* (1999).

Additionally, experimental and theoretical work regarding imbibition has examined the scaling aspects of the process in order to estimate oil recovery from reservoir matrix blocks that have shapes and sizes different for those of laboratory core samples (Handy, 1960; Morrow *et al.*, 1994; Ma *et al.,* 1995; Cil and Reis, 1996; Garg *et al.*, 1996; Zhang *et al.*, 1996; Bourbiaux *et al.*, 1999; Reis and Cil, 1999; Zhou *et al.*, 2001). Handy (1960) in describing air/water systems stated that imbibition could be described by either a diffusion-like equation or a frontal-advance equation, depending on assumptions. However, both solutions predict that the mass of water imbibed depends linearly on the square root of time in one-dimensional media. This has been verified by numerous other studies (Akin *et al.*, 2000; Cil and Reis, 1996; Reis and Cil, 1993; Reis and Haq, 1999; Rangel-German and Kovscek, 2000(a,b); Li and Horne, 2000). In the case of oil, a number of experimental results for oil recovery in fractured media have been reported in the literature (Kazemi *et al.*, 1989; Mattax and Kyte, 1962). Reis and Cil (2000) concluded that the best models for the early-time period in one-dimensional flow are the square-root of time and the so-called "linear-saturation-profile" models. They proposed an empirical power-law-based model for the late-time period. This last model cannot be extrapolated to early-time periods.

Other studies have applied rigorous mathematical analyses to model pore-scale imbibition to find ultimately matrix-fracture transfer functions for naturally fractured reservoirs (Bourbiaux, 1999; Reis and Cil, 2000; Reis and Haq, 1999). In related work, Hughes and Blunt (2001) developed a network model to simulate imbibition and multiphase flow in fractures. They compute realistic-looking multiphase saturation distributions using the measured fracture aperture distribution of a rough fracture. Such methodology should prove useful in understanding the relative permeability behavior of fractures.

The above studies largely focused on the mechanisms dominant in gravity drainage situations, imbibition displacements in one-dimensional media, and/or have emphasized understanding flow through a single fracture with no transfer to the matrix. It is readily clear that capillary imbibition is an important mechanism in fractured porous media and that further study regarding matrix-fracture mass transfer, as well as on multiple fracture systems, is needed.

3. Experimental Design and Procedure

Our experimental design originates from the ideas displayed in Fig. 1. Where initial water saturation is low, results (*e.g.*, Akin *et al.*, 2000) have shown in one-dimensional media that there is a well-defined spreading front parallel to the surface exposed to the imbibing fluid. This fluid advances at a speed proportional to the square root of time, as shown in Fig. 1a. This is the basis for the so-called "square root of time models" of imbibition. Assume that the same physical process occurs in all directions in multidimensional porous media, even against the force of gravity. Next, consider a two-dimensional medium where water imbibes from a stationary line source, as shown in Fig. 1b. It is apparent that the progress of water imbibition in the x-direction is proportional to the square root of time, and, likewise, in the z-direction. Thus, in two-dimensional media, the overall mass of water imbibed is proportional to the product of the extent of imbibition in each direction. Imbibition in this case should scale linearly with time. Later, this is shown to be true experimentally. Finally, this analysis suggests that three-dimensional water imbibition from a point source scales with time to the three-halves power, Fig. 1c.

3.1 Coreholder

A novel experimental set-up was designed to insure minimal artifacts while imaging and the collection of maximum saturation information. It is described next.

Due to the cubic geometry of the cores and our desire to measure in-situ saturations with X-ray CT, conventional core holders could not be used. A novel, CT-compatible imbibition coreholder was designed. Figures 2 and 3 present the apparatus schematically. The basic idea is to avoid drastic changes of density of the object scanned by presenting circular cross-sections to the scanner. We initially coated and sealed the outside surface of the Berea sandstone (Cleveland Quarries) samples with Marine Epoxy (Tap Marine Plastic #314). The cores were then potted in vertical cylindrical PVC containers with the same epoxy. Once the core was epoxied in the PVC container, the bottom face of the cylinders was cut open to expose rock. Sufficient core was removed so that no trace of epoxy remained on this face. Subsequent CT scans of the core verified this statement.

This PVC core-holder was placed in a second horizontal cylindrical acrylic container, as shown in Fig. 2. We used a cylindrical shape to allow the core to be rotated in any position around the horizontal axis. Once filled with water, the second container works as a water jacket to lessen the contrast in density between the acrylic and PVC/epoxy and to achieve some measure of temperature control. Thus, the cross-sectional shape for scanning is symmetric and circular improving image quality. The scanning plane is the cross section shown in Fig. 2.

Acrylic end-caps were machined to mate with the circular PVC core-holder. The end caps have 2 perforations (inlet and outlet) to give planar 2D flow across the face of the block. The end-caps (one at the top and one at the bottom) were attached to the PVC coreholder by means of through bolts and sealing O-rings. Fracture apertures were set by means of metallic shims (essentially feeler gauges of precise thickness) placed between the block and end-cap. Thus, a uniform fracture aperture is guaranteed along the entire core. With this system, we inject and produce fluids in any combination desired. The end-caps are also shaped so that core and end-caps fit the inner diameter of the water jacket when assembled. This combination of end-caps, core, and water jacket allowed us to set repeatedly the coreholder in a unique position. We compare identical cross sections from experiment to experiment.

In summary, Figures 2 (front view) and 3 (top view) show a diagram of the coreholder used in this work. We found that this set-up reduces X-ray artifacts and improves significantly the resolution of CT images. The key to obtaining flat artifact-free images is the circular cross-sectional shape presented to the scanner.

3.2 CT Scanner

A CT Scanner is used here to measure porosity, saturation, and to track advancing fronts. It can also be used to measure fracture apertures (Hunt *et al.*, 1987; and Johns *et al.*, 1993). Both static and dynamic experiments can be monitored using a CT scanner. Dynamic experiments, such as corefloods, follow the change in CT numbers with position and time. The timing of these experiments is more crucial.

The CT Scanner utilized in this work is a Picker 1200SX Dual Energy CT scanner. It is a fourth generation medical scanner that is now used solely for laboratory purposes. Most CT scanners measure linear attenuation coefficient, with a cross-sectional resolution less than 1 mm. Voxel dimensions in this work are 0.5 mm by 0.5 mm by 8 mm thick. The most important aspect in CT use is good image quality. Image artifacts affect the results of subsequent saturation calculations. Two aspects affect image quality, the experimental design and the machine parameters. In terms of machine parameters, the best quality resolution as well as the optimum parameters were selected by trial and error. Table 1 shows the scanner settings used in this work. Relevant settings include a field size of 16 cm, high resolution, slice thickness of 8 mm, tube current and voltage at 80 mA and 130 kV, respectively.

3.3 Positioning System

The positioning system consists of a translating table equipped with a stepper motor (Compumotor, RP240, Parker Hannifan Co.) Positioning is accomplished electronically with ±0.01mm accuracy. Basically, any flat surface can be attached to this table using bolts. An L-shaped device that attached to the moving table and that holds the core-holder in a fixed position was built.

3.4 Pump and Fluids

A positive displacement Constametric 3200 (LDC Analytical) pump was calibrated and used. This pump delivers 0.10 to 9.99 cm^3/min in 0.01 cm^3/min increments. For very low flow rate experiments, an Isco 500 D (Instrumentation Specialties Co.) syringe pump is employed.

CT numbers of fluids are proportional to their densities. For instance, water has a CT number of 0, while air is -1000. Castanier (1990) found that adding salts such as KI or NaBr to the water helps to improve the measurement of fluid saturations essentially by improving contrast. Demiral (1991) found that CT number can be increased dramatically by increasing the concentration of dopant. A selection of fluids and dopant were sampled in order to obtain the best contrast in CT numbers, so that phases could be easily recognized in the images. Decane was used to represent the oil phase, 5% NaBr by weight brine solution for the water phase, and air for the gas phase. Pure fluid CT numbers were measured because their values are needed for the saturation calculations. The CT numbers as well as some fluid properties are shown in Table 2.

3.5 Experimental Procedure

Prior to each experiment, cores were dried to zero water saturation in a vacuum oven. The core holder was assembled and the fracture aperture set. A number of experiments at constant water injection rates into the fracture were performed. Injection rates varied from very low to very high (0.1 cc/min to 4 cc/min). We also used different fracture apertures, going from very narrow (0.025mm) to wide (0.1 mm). Setting the flow rate and having fixed the fracture thickness, we obtained CT images to observe the progress of multidimensional imbibition. For the experiments reported here, water was injected on the left and produced from the right-hand side. The idea was to have uniform advance of water along the bottom face of the core. Once the injection started, the core was scanned at the same location for successive times.

Most of the experiments conducted here involved water and air. This system gives easily reproducible results in a relatively short period of time. Rather than conduct a few long experiments, we deemed it preferable to conduct many shorter experiments that allow us to examine a wide range of conditions. In the case of experiments with oil, CO_2 was first injected into the system and this was followed with oil. The CO_2 is relatively soluble in oil and the

combination allowed the system to be fully saturated with oil. Water and air saturations were calculated from the CT images as:

$$S_w = \frac{CT_{aw} - CT_{cd}}{CT_{cw} - CT_{cd}} \tag{1}$$

where CT_{aw} is the CT number for water and air saturated core at a voxel location, CT_{cd} is the CT number for the dry core at a voxel location, and CT_{cw} is the CT number for a 100% water saturated voxel. Similarly, for oil-water systems:

$$S_w = \frac{CT_{ow} - CT_{cw}}{\phi(CT_o - CT_w)} \tag{2}$$

where CT_{ow} is the CT number for a water and oil saturated core at a voxel location, CT_o is the CT number for the oil phase, CT_w refers to the water phase, and ϕ is the independently measured porosity of a voxel. The CT number for oil (decane) is around -280, as shown in Table 2.

For this work, all sandstone samples were 5 x 5 x 5 cm blocks. Porosity was calculated from CT images according to (Withjack, 1998)

$$\phi = \frac{CT_{cw} - CT_{cd}}{CT_w - CT_a} \tag{3}$$

where CT_a is the CT number for air. Figure 4 shows the porosity distribution of one volume section of the rock calculated with Eq. 3. The average porosity is 25% and the distribution is relatively narrow (standard deviation = 2%) indicating homogeneity.

4. Experimental Results

Following the aforementioned procedure, experiments were conducted at a variety of flow rates and fracture apertures for the air-water system. Figures 5 and 6 display typical results and illustrate the presence of two different fracture-flow regimes. Both images were taken after 0.32 PV of water had imbibed into the core. White shading indicates water and black shading indicates air. Both systems have an injection rate into the fracture of 1cc/min. The chief difference between the two experiments is the fracture aperture. A wide fracture of 0.1 mm (Fig. 5) leads to relatively slow water advance through the fracture and a two-dimensional imbibition pattern. On the other hand, the fracture fills with water quickly when the aperture is narrow, 0.025 mm. As shown in Fig. 6, the imbibition pattern is one-dimensional in this case.

4.1 "Filling-Fracture" Regime

This regime shows a variable length plane source due to relatively slow water flow through fractures. Water horizontal advance is controlled by the interaction between the matrix and the fracture as shown in Figs. 5 and 7. Because the advance of water in the horizontal and vertical directions each scale linearly with the square root of time, we anticipate that the mass of water imbibed scales linearly with time. That is, the mass imbibed in this two-dimensional geometry is proportional to the product of these two length scales.

CT images were obtained throughout the duration of injection and they allow us to analyze the progress of imbibition, as shown in Fig. 7. Again, dark shading indicates zero water saturation while white indicates fully water saturated. From these saturation fields, we also obtain the average water saturation, $\overline{S_w}$, as a function of time. Average water saturation is, of course, linearly proportional to the mass of water imbibed and nonwetting fluid expelled. Because of the low density of air and the matrix/fracture geometry oriented opposite to the direction of gravity, we found that the trapped gas saturation, 38%, is relatively high. Fig. 8 summarizes the "filling-fracture" portion of all air-water experiments conducted. Within experimental uncertainty, the mass imbibed scales linearly with time before the advancing water front reaches the end of the fracture. Note also, Fig. 8 reports an experiment where the initial water saturation was about 0.22. The rate of imbibition is less because capillary forces are weaker than the cases with zero initial water saturation; however, a linear relationship between the mass of water imbibed and time is apparent.

4.2 "Instantly-Filled" Regime

In this regime, little water imbibes before the fracture fills with water. The image in Fig. 6 is nearly one-dimensional water advance. We expect the mass of water imbibed to scale linearly with the square root of time. Figure 9 summarizes the results obtained for all water-air experiments in the "instantly-filled" regime. Very early-time behavior is within the "filling-fracture" regime above. At later times, and within experimental uncertainty, the mass imbibed scales linearly with the square root of time. Results are all highly repeatable and the residual nonwetting phase saturation varies between 0.38 and 0.42. The behavior of this second regime is very similar to that observed during both counter current and cocurrent imbibition experiments reported previously in the literature (Akin *et al.*, 2000; Handy, 1960; Cil and Reis, 1996; Reis and Cil, 1999; Reis and Haq, 1999; Rangel-German and Kovscek, 2000(a,b)); Li and Horne, 2000, Zhou *et al.*, 2001). Note, here imbibition is strictly counter current in a macroscopic sense because all sides except the bottom face are sealed.

4.3 Oil-Water System

A number of experiments were conducted with n-decane and brine to generalize results from the air-water experiments. We examined both the instantly-filled and filling-fracture regimes. In the next section, we will develop a predictive model delineating parameters leading to either instantly-filled or filling-fracture regimes. Two orientations of the apparatus were used. In the first, the fracture was oriented horizontally at the bottom of the matrix, exactly as above.

In the second, the fracture was placed on top of the matrix. This was done to examine the role of gravity and, thus, to explain the relatively high residual gas saturation in the air-water experiments. An injection rate of 0.5 cm^3/min and a fracture aperture of 0.1 mm are used to obtain instantly filled fractures, whereas 0.1 cm^3/min and 0.025 mm are used to examine the filling-fracture regime.

Figure 10 shows the average water imbibed versus the square root of time. The two cases with a 0.1-mm fracture aperture and 0.5 cm^3/min flow rate (one in the direction of and the other opposed to gravity) are obviously linear with respect to $t^{1/2}$ for a substantial period of time, as expected for instantly-filled fractures. The effect of gravity on the orientation of the fracture/matrix combination is also evident. Total water imbibed and oil recovery rates are greater at virtually all times when the fracture is placed on top of the matrix.

These two curves do not display any filling-fracture behavior as was found at very small times in Fig. 9. The first reason for this result is that the rate of matrix-fracture transfer is less in the oil-water system. Capillary forces are relatively weaker because the oil-water interfacial tension is less than that for air-water. Also slowing matrix-fracture transfer is the fact that the oil-phase is viscous and not as easily displaced as air. A second reason is that the water injection rate is simply high. The time to fill fractures is substantially less than the total time of the experiment.

In order to examine the filling-fracture regime for the oil-water system, a flow rate and fracture aperture of 0.1 cm^3/min and 0.025 mm, respectively, are used. As during the air-water experiments, CT images were obtained throughout the duration of water injection, and they allow us to analyze the progress of imbibition for oil-water systems, as shown in Fig. 11. Again, dark shading indicates zero water saturation while white indicates full water saturation. The curve corresponding to this experiment in Fig. 10 displays filling-fracture behavior for early times. One can see that the fracture must fill with water before the behavior of the curve is linear with respect to $t^{1/2}$. The early filling-fracture regime for oil-water systems also follows a linear relationship with time as we saw in the air-water experiments.

From the observations summarized in Figs. 5 to 11, we establish that imbibition behavior can be approximated by means of the square root of time model for the "instantly-filled fracture" system. For fracture systems where the water advance is relatively slow, imbibition advances linearly with respect to time and a new model is required. Additionally, once imbibing water reaches the upper boundary of the core, the system no longer behaves in a semi-infinite fashion. This very late-time regime is neither proportional to $t^{1/2}$ nor t.

5. Analytical Model for Imbibition

This section develops a model for early-time behavior while water is advancing in the fracture. The "instantly-filled" regime is well described by the square-root-of-time model and so is not reanalyzed here. Sets of images such as those shown in Fig. 7, obtained for different times, are used to analyze the progress of multi-dimensional imbibition. For instance, we obtain a set of images where the shape and position of the front of the iso-saturation curve for S_{wmax} (62%, for the experiments reported here) is tracked.

We pursued an analytical model to describe the amount of water transfer into the matrix so that matrix/fracture transfer functions and the shape factors necessary for numerical simulation can be formulated later. The imbibition process is approximated by a diffusion-like equation with a capillary-pressure-based hydraulic diffusivity. We assumed: 1) the water saturation in the matrix is constant initially, 2) the water saturation in the matrix at an infinite distance from the fracture remains constant, and 3) the convection/diffusion equation with constant diffusivity, α_h, applies for this problem. For a one-dimensional geometry, this is written as

$$\alpha_h \frac{\partial^2 S_w}{\partial z^2} - u\frac{\partial S_w}{\partial z} = \phi \frac{\partial S_w}{\partial t} \tag{4}$$

where $\alpha_h = kk_{rw}/\mu_w\,(dP_c/dS_w)$ and z is the vertical direction. The boundary conditions are

$$S_w(z,0) = \text{constant} \tag{5}$$

$$S_w(0,t) = S_{wmax} \tag{6}$$

$$\lim_{z\to\infty} S_w(z,t) = \text{constant} \tag{7}$$

Above, S_w is the water saturation, z is the vertical distance from the fracture, t is the time, and u is the interstitial velocity. The solution to this equation is commonly obtained by means of the Laplace transform.

Upon neglecting convection in the matrix (u = 0), the 1-D solution of the diffusion equation subject to these boundary conditions is (Carslaw and Jaeger, 1959)

$$S_w(z,t) = erfc\left(\frac{z}{2\sqrt{\alpha_h t}}\right) \tag{8}$$

A linear superposition of Eq. 8 in the (horizontal) x-direction approximates the S_w distribution obtained in the matrix within the "filling-fracture" regime. Matrix is not allowed to fill until the time, τ, when a front within the fracture reaches a particular x position. The implications of this assumption are discussed further below. Another necessary approximation is to treat matrix/fracture transfer analytically. Knowing the horizontal position of the front, which is obtained analytically in the following section, and using Eq. 8 with an estimated value for hydraulic diffusivity (Rangel-German and Kovscek, 2000 (a,b)), we can calculate the vertical position of any iso-saturation, S_w, we desire.

It is not simple to obtain the location of the water front in the fracture. Mass transfer between the fracture and the matrix slows the frontal advance within the fracture. In order to obtain the location of the front in the fracture, we used a material balance, as shown in Eq. (9), and assumed that water and the rock are incompressible:

$$q_{w,inj} = q_{w,m} + q_{w,f} \tag{9}$$

where $q_{w,inj}$ is the volumetric water injection rate, $q_{w,m}$ is the volumetric rate at which water enters the matrix, and $q_{w,f}$ is volumetric water advance rate in the fracture. Equations (10) and (11) give the water transfer rate from the fracture to the matrix, $q_{w,m}$, and the fracture width that can be filled by water, respectively

$$q_{w,m} = 2n \int_0^t \left(\alpha_h \left. \frac{\partial S_w(z, t-\tau)}{\partial z} \right|_{z=0} \frac{dA(t)}{d\tau} \right) d\tau \tag{10}$$

$$w_{w,f} = n\phi_f w_f \tag{11}$$

where n is the number of fractures associated with the matrix block, ϕ_f is the fracture porosity, w_f is the fracture width, A is the area of the matrix exposed to wetting fluid and τ is the time when a portion of the fracture surface is exposed to water. The factor 2 appears in Eq. (10) because a fracture is, generally, bounded by 2 matrix blocks. The water advance in the fracture is given as

$$q_{w,f} = n\phi_f w_f \frac{dA}{dt} \tag{12}$$

Upon substitution and simplification with Eqs. (9) to (12), we obtain:

$$q_{w,inj} = 2n \int_0^t \left[\alpha_h \left. \frac{\partial S_w(z, t-\tau)}{\partial z} \right|_{z=0} \right] \left(\frac{dA}{d\tau} \right) d\tau + n\phi_f w_f S_{w\max} \frac{dA}{dt} \tag{13}$$

Equation (13) is the material balance equation written in terms of the water transfer rate to the matrix and the areal extent of water advance in the fracture. We solved Eq. (13) for A(t) by substituting the Laplace transform with respect to time of Eq. (8) into the Laplace transform with respect to time of Eq. (13). Equations (14) and (15) show the Laplace transforms of Equations (8) and (13), respectively.

$$\left. \frac{\partial S_w(z, s)}{\partial z} \right|_{z=0} = \frac{S_{w\,max}}{\sqrt{s\alpha_h}} \tag{14}$$

$$\frac{q_{w,inj}}{s} = 2n \left\{ \alpha_h \left. \frac{\partial S_w^*(z,s)}{\partial z} \right|_{z=0} \right\} \left[sA^*(s) - A^*(0) \right] + n\phi_f w_f S_{w\max} \left[sA^*(s) - A^*(0) \right] \tag{15}$$

where S^*_w and A* are the Laplace transform of the water saturation (S_w) and the area filled with water in the fracture (A), respectively. Substituting Eq. (14) into Eq. (15) and making A*(0) = 0, because the area filled with water at time zero, A(0), is equal to zero, results in

$$\frac{q_{w,inj}}{s} = 2n \left\{ \phi \frac{\sqrt{\alpha_h}}{\sqrt{s}} S_{w\max} \right\} sA^*(s) + n\phi_f w_f S_{w\,max} sA^*(s) \tag{16}$$

Solving for A*(s):

$$A^*(s) = \frac{q_{w,inj}}{nsS_{wmax}} \frac{1}{\left[2\phi\sqrt{\alpha_h s} + \phi_f w_f s\right]} \tag{17}$$

Applying the Laplace back-transform, the solution for the area of the fracture filled with water, in time space is

$$A(t) = \frac{q_{w,inj}\phi_f w_f}{4n\alpha_h\phi^2}\left\{e^{t_D} erfc\left[\sqrt{t_D}\right] + 2\sqrt{\frac{t_D}{\pi}} - 1\right\} \tag{18}$$

where

$$t_D = 4\left(\frac{\phi}{\phi_f}\right)^2 \frac{\alpha_h}{w_f^2} t \tag{19}$$

Finally for a block of constant width normal to flow, the expression for the frontal advance in the fracture, X(t), incorporating imbibition of wetting fluid into the matrix is

$$X(t) = \frac{A(t)}{W} = \frac{q_{w,inj}\phi_f w_f}{W4n\alpha_h\phi}\left\{e^{t_D} erfc\left[\sqrt{t_D}\right] + 2\sqrt{\frac{t_D}{\pi}} - 1\right\} \tag{20}$$

where W is the width of the block.

6. Discussion

Equation (20) is similar to that obtained by Marx and Langenheim (1959) for the areal extent of an equivalent heated zone in thermal recovery. Rearranging terms, the analogy between heat transfer and flow in fractured porous media is apparent. These terms are shown in Table 3. The fracture is equivalent to the reservoir zone where hot fluid is injected, whereas the matrix is equivalent to the overburden. The linear superposition of Eq. (8) to obtain the distribution of water in the matrix is, thus, similar to calculation of the overburden heat losses in the Marx and Langenheim method. Prats (1969; 1986) showed that linear superposition of the 1-dimensional heat conduction equation to calculate overburden heat losses gave excellent approximation of the rigorous solution. Because of the similarity between heat and mass transfer, we expect that superposition of Eq. (8) well represents the transfer of fluid from the fracture to the matrix.

Our experimental results have shown that the "filling-fracture" regime has a linear relationship with time, whereas the "instantly-filled fracture" regime has a linear relationship with the square root of time. The analytical model also displays these time dependencies and predicts the critical time separating “filling” and “instantly-filled” regimes.

The characteristic time, t_c, is the boundary between imbibition regimes. It can be found implicitly from Eq. (20) when X is set to the fracture characteristic length. For example, with the parameters used for the calculations in Fig. 12, t_{Dc} equals 1800 and in dimensional quantities t_c

equals 12.5 min. This compares favorably with the air-water experimental results in Fig. 7 where the critical time is between 10 and 15 min. Also note that the calculations well represent the shape and velocity of the water front.

The term $2\sqrt{(t_D/\pi)}$ in Eq. (18) dominates the term inside the bracket for large t_D (>50). Using only this term is a very good approximation, resulting in the following expressions for the area filled with water and 'filling-fracture' rate:

$$A(t) = \frac{q_{w,inj}}{n\phi}\sqrt{\frac{t}{\pi\alpha_h}} \qquad t \le t_c \tag{21}$$

Eq. (21) shows the apparent direct relationship between frontal advance in the fracture (x-direction) with square-root of time. Imbibition in the z-direction is also proportional to the square root of time. Hence, the total fluid imbibed is linear with respect to time.

The difference between the areas under the curves in Fig. 12 is directly proportional to the mass of water imbibed in the elapsed time between t_1 and t_2. Thus, the value of the rate of imbibition for the "filling-fracture" regime, R_{ff}, can be calculated as

$$R_{ff} = \frac{\partial \overline{S_w}}{\partial t} = lim_{\Delta t \to 0} \frac{\phi}{A_T} \frac{\iint S_w(X,Y,t_2)dx_D dy_D - \iint S_w(X,Y,t_1)dx_D dy_D}{\Delta t}$$

$$= R_{ff} = q_{w,inj}\left(1 - e^{t_D} erfc\left[\sqrt{t_D}\right]\right) \qquad t_c \le t \tag{22}$$

R_{ff} is a constant for a given set of constant injection rate, fracture aperture, and fluid systems. We can also write the material balance, Eq. (9), as

$$Q_m(t) = q_{w,inj}t - Q_{w,f} \tag{23}$$

where Q_m is the volume of water imbibed to the matrix and $Q_{w,f}$ is the volume of water in the fracture. Then

$$R_{ff} = \frac{dQ_m(t)}{dt} = q_{w,inj} - q_{w,f} \qquad t \le t_c \tag{24}$$

where $q_{w,f}(t)$ is given by Eq. (12) and dA(t)/dt (in Eq. 12) is the derivative of Eq. (18). Substituting in Eq. (24):

$$R_{ff} = q_{w,inj}\left(1 - e^{t_D} erfc\left[\sqrt{t_D}\right]\right) \tag{25}$$

We note that the "instantly-filled" regime is well described by Eq. (8) and needs no further analysis. Thus for both regimes and accounting for initial water saturation, S_{wi}, the equation for average water saturation in the matrix block is:

$$\overline{S_w} = t\,R_{ff}\left[1 - H(t-t_c)\right] + \left[t_c\,R_{ff} + (t-t_c)^{0.5}\,R_{if}\right]H(t-t_c) + \overline{S_{wi}} \tag{26}$$

where H is the Heaviside function; and t_c is the characteristic time for the fracture. The characteristic time, t_c, is the boundary between both regimes. The fracture fills instantly with respect to the matrix if t_D (= t/t_c) is large.

7. Conclusions

An experimental apparatus was built that allows detailed and accurate measurement of the extent and rate of imbibition in an idealized fracture and matrix block. With the novel coreholder, a single X-ray CT exposure is used to image the entire length of the matrix block and the matrix/fracture interface. The spatial distribution of water measured with respect to time explains the observed trends in imbibition behavior. Importantly, the existence of two different modes of matrix and fracture fill-up are found. Relatively slow flow through fractures is found when fracture to matrix fluid transfer is relatively rapid, fracture aperture is wide, and/or water injection is slow. In this regime, fractures fill slowly with fluid and we refer to the behavior as a "filling fracture". Recovery scales linearly with time. On the other hand, relatively low rates of fracture to matrix transfer, narrow apertures, and/or high water injection rates lead to rapid flow through fractures. We term this regime "instantly filled" and recovery scales with the square-root of time.

The relatively simple analytical model described here was validated with the experimental data. The water saturation pattern within matrix blocks, the linear scaling of recovery with respect to time in the "filling-fracture" regime, and the growth of wetted fracture with respect to the square-root of time are well reproduced by the model. In the limit of an "instantly-filled" fracture, the theory reduces to the well known square-root-of-time model for imbibition performance. Importantly, it provides a means to calculate the critical time differentiating filling and instantly-filled fracture flow regimes. Of course, the model also allows us to estimate the results of imbibition in matrix/fracture systems different than those explicitly examined.

8. Nomenclature

A	=	area (m^2)
CT	=	CT number (Hounsfields)
H	=	Heaviside function
k	=	absolute permeability (m^2)
k_r	=	relative permeability
n	=	number of fractures
P_c	=	capillary pressure (Pa)
Q	=	rate (m^3/s)
R	=	rate of imbibition (m^3/s)
S	=	saturation
t	=	time (s)
u	=	velocity (m/s)
W	=	fracture width (m)
x	=	horizontal distance(m)

X	=	location of wetting fluid front in fracture (m)
z	=	vertical distance (m)

Greek

α_h	=	hydraulic diffusivity (m^2/s)
ϕ	=	porosity
μ	=	viscosity (Pa-s)

subscripts/superscripts

aw	=	air-water
cd	=	dry core
c	=	critical
cw	=	water-saturated core
D	=	dimensionless
f	=	fracture
ff	=	filling fracture
if	=	instantly filled
inj	=	injected
m	=	matrix
o	=	oil
ow	=	oil-water
w	=	water
*	=	variable in Laplace space

References

Akin, S., Schembre, J.M., Bhat, S.K., and Kovscek, A.R.: "Spontaneous Imbibition Characteristics of Diatomite," Journal of Petroleum Science and Engineering, 25: 149-165, 2000.

Bourbiaux, B., Granet, S., Landereau, P., Noetinger, B., Sarda, S., and Sabathier, J.C.: "Scaling Up Matrix-Fracture Transfer in Dual-Porosity Models: Theory and Applications" SPE56557, presented at the SPE Ann. Tech. Conf. and Exhibition, Houston, TX, 3-6 Oct., 1999.

Carslaw H.S., and Jaeger J.C.: "Conduction of Heat in Solids," Oxford Science Publications, Oxford University Press Inc., 1959.

Castanier, L.M.: "An Introduction to Computerized X-Ray Tomography for Petroleum Research," SUPRI TR-66, Stanford University, May 1990.

Cil, M. and Reis, J.C.: "A Multi-Dimensional, Analytical Model for Counter-Current Water Imbibition into Gas-Saturated Matrix Blocks," J.Pet. Sci & Eng., **16**: 61-69, 1996.

Cil, M., Reis, J.C., Miller, M.A., and Misra, D.: "An Examination of Countercurrent Capillary Imbibition Recovery from Single Matrix Blocks and Recovery Predictions by Analytical Matrix/Fracture Transfer Functions," presented at the SPE Ann. Tech. Conf. And Exhibition, New Orleans, LA, 27-30 Sept., 1998.

Demiral, B.: "Three Dimensional Laboratory Steam Injection Model," SUPRI Heavy Oil Research Program, Fourteenth Annual Report, Stanford, California, June, 1991.

Garg, A., Zwahlen, E., and Patzek, T.W.: "Experimental and Numerical Studies of One-Dimensional Imbibition in Berea Sandstone," Proceedings of the Sixteenth Annual American Geophysical Union Hydrology Days, Fort Collins, CO, 15-18 April, 1996.

Handy, L.: "Determination of Effective Capillary Pressure for Porous Media from Imbibition Data." Pet. Trans. AIME **219**: 75-80, 1960.

Hughes, R.G.: "CT Measurements of Two-Phase Flow in Fractured Porous Media," MS Report, Stanford University, Stanford, CA, 1995.

Hughes, R.G. and Blunt, M. J.: "Network Modeling of Multiphase Flow in Fractures," Advances in Water Resources 24(3,4): 409-421, 2001.

Hunt, P.K., Engler, P., and Bajsarowicz, C.: "Computed Tomography as a Core Analysis Tool: Applications and Artifact Reduction Techniques", SPE16952, presented at the SPE Ann. Tech. Conf. and Exhibition, Dallas, TX, 27-30 September, 1987.

Johns, R.A. Steude, J.S., Castanier, L.M., and Roberts, P.A.: "Nondestructive Measurements of Fracture Aperture in Crystalline Rocks Using X-ray Computed Tomography," Journal of Geophysical Research 98: 1889-1900, 1993.

Jones, T. A., Wooten, S. O., and Kaluza, T. J.: "Capillary Continuity Between Blocks of a Fractured Reservoir," paper SPE 20515 presented at the SPE Ann. Tech. Conf. and Exhibition, New Orleans, LA, 23-26 September, 1990.

Kazemi, H., Gilman, J.R.: "Multiphase Flow in Fractured Petroleum Reservoirs," in Flow and Contaminant Transport in Fractured Rock, Bear, J.R., Tsang, C. F., and de Marsily, G (eds.), Academic Press, San Diego, CA, 267-323, 1993.

Kazemi, H., Gilman, J.R., and El-Sharkaway, A.M.: "Analytical and Numerical Solution of Oil Recovery from Fractured Reservoirs Using Empirical Transfer Functions." SPE19849, presented at the SPE 64th Ann. Tech. Conf. And Exhibition, San Antonio, TX, 8-11 Oct., 1989.

Li, K. and Horne, R.: "Characterization of Spontaneous Imbibition into Gas-Saturated Rocks" SPE62552, presented at the SPE/AAPG Western Regional Meeting, Long Beach, California, 19-23 June, 2000.

Ma, S., Morrow, N.R., and Zhang, X.: "Experimental Verification of a Modified Scaling Group for Spontaneous Imbibition." SPE 30762, presented at the SPE Ann. Tech. Conf. And Exhibition, Dallas, TX 22-25 Oct., 1995.

Marx, J. W. and Langenheim, R. H.: "Reservoir Heating by Hot Fluid Injection,"Trans.,AIME(1959)**216**, 312-315.

Mattax, C., and Kyte, J.R.: "Imbibition Oil Recovery from Fractured Water-Drive Reservoirs." Soc. Pet. Eng. J. **2**: 177-184, 1962.

Mogensen, K., and Stenby, E.H.: "A Dynamic Two-Phase Model Pore-Scale Model of Imbibition," Transport in Porous Media, **32**: 299-327, 1998.

Morrow 1994. Morrow, N.R., Ma, S., Zhou, X., and Zhang, X.: "Characterization of Wettability from Spontaneous Imbibition Measurements." CIM 94-475, presented at the 45th Ann. Tech. Meeting of the Pet. Soc. Of the CIM, Calgary, Alberta Canada, 12-15 Jun., 1994.

Pan, X. and Wong, R.C.: "Steady State Two-phase in a Smooth Parallel Fracture," presented at the 47th Annual Technical Meeting of The Petroleum Society in Calgary, Alberta, Canada, June 10-12, 1996.

Persoff, P. and Pruess, K.: "Two-Phase Flow Visualization and Relative Permeability Measurement in Natural Rough-Walled Rock Fractures," Wat. Res. Res. 31: 1175-1186, 1995.

Pooladi-Darvish, M. and Firoozabadi, A.: "Cocurrent and Countercurrent Imbibition in a Water-Wet Matrix Block," Soc. Pet. Eng. J. **5**: 3-11, 2000.

Prats, M.: "The Heat Efficiency of Thermal Recovery Projects," Trans. AIME 246: 323-332, 1969.

Prats, M.: Thermal Recovery, 2nd Printing, Society of Petroleum Engineers, Dallas, TX, 43-45 (1986).

Rangel-German, E.: " Experimental and Theoretical Investigation of Multiphase Flow in Fractured Porous Media," MS report, Stanford University, Stanford, CA, 1998.

Rangel-German, E., Akin, S., and Castanier, L.: "Multiphase-Flow Properties of Fractured Porous Media," SPE 54591 presented at the SPE Western Regional Meeting, Anchorage, AK, 26-28 May, 1999.

Rangel-German, E. and Kovscek, A.: "Matrix-Fracture Interaction in Single Matrix Blocks," presented at Twenty-fifth Workshop on Geothermal Reservoir Engineering, Stanford University, Stanford, CA, January 24-26, 2000.

Rangel-German, E. and Kovscek, A., "Experimental and Analytical Study of Water Infiltration in Fractured Systems," presented at the Annual Geothermal Resources Congress, San Francisco, USA. September, 2000.

Reis, J.C. and Cil, M.: "A Model for Oil Expulsion by Counter-Current Water Imbibition in Rocks: One-Dimensional Geometry," J. Pet. Sci & Eng., **10**: 97-107, 1993.

Reis, J. and Cil, M.: "Analytical Models for Capillary Imbibition: One-Dimensional Matrix Blocks." In Situ, **23(3)**, 243-270, 1999.

Reis, J.C. and Haq, S.A.: "Water Advance in a Single Fracture in the Presence of Capillary Imbibition into Adjacent Matrix Blocks." In Situ, **23(3)**, 271-295, 1999.

Reis J, Cil M.: "Analytical models for capillary imbibition: Multidimensional matrix blocks." In Situ, **24(1),** 79-106, 2000.

Romm, E. S.: *Fluid Flow in Fractured Rocks*, Nedra Publishing House, Moscow (1966).

Saidi, A. M.: "Simulation of Naturally Fractured Reservoirs," SPE 12270 presented Symposium on Reservoir Simulation, San Francisco, CA, 16-18 November, 1983.

Whitherspoon, P. A., Wang, J. S., Iwai, K., and Gale, J. E.: "Validity of the Cubic Law for Fluid Flow in a Deformable Rock Fracture," *Water Resources Research, Vol. 16, No. 6* (1980) 1016-1024.

Withjack, E.M.: "Computed Tomography for Rock-Property Determination and Fluid-Flow Visualization", SPEFE (December 1988) 696-704

Zhang, X., Morrow, N.R., and Ma, S.: "Experimental Verification of a Modified Scaling Group for Spontaneous Imbibition." Soc. Pet. Eng. Res. Eng. **11**: 280-285, 1996.

Zhou, D., Jia, L., Kamath, J. and Kovscek, A. R.: "Scaling of Counter-Current Imbibition Processes in Low-Permeability Porous Media," Journal of Petroleum Science and Engineering, to appear, 2001.

TABLE 1. CT SCANNER SETTINGS	
Parameter	Setting
Field of View	**16 cm**
Image Matrix	**1024 x 1024**
Sampling	**1024**
Scan Speed	**3 sec**
Slice Thickness	**8 mm**
Resolution	**High**
Kv	**130**
MA	**80**
x-ray filter	**3**
MAS	**341 per slice**
Exposure	**5.09 sec/slice**
Pilot	**0.00 sec**

TABLE 2. FLUID PROPERTIES				
Property	**5% NaBr Solution**	**Water**	**Decane**	**Air**
Specific Gravity	**1.001**	**1.0**	**0.73421**	**0.0012**
Viscosity	**1.075 cp**	**1.0 cp**	**0.95**	**~0.02 cp**
CT Number	**~ 350**	**0**	**~ -280**	**~ -1000**

TABLE 3. ANALOGOUS TERMS BETWEEN HEAT TRANSFER AND FLOW IN FRACTURED POROUS MEDIA	
Fluid flow in Fractured Porous Media	**Heat transfer in Porous Media**
$q_{w,inj}$, constant water injection	**q_i, constant rate of heat injection**
ϕ, porosity of the matrix	**M_s, volumetric heat capacity of overburden**
ϕ_f, porosity of the fracture	**M_R, volumetric heat capacity (reservoir)**
α_h, hydraulic diffusivity	**α_s, thermal diffusivity**
w_f, fracture width (aperture)	**h_t, gross thickness**
ΔS_w, saturation difference	**ΔT_i, temperature difference**

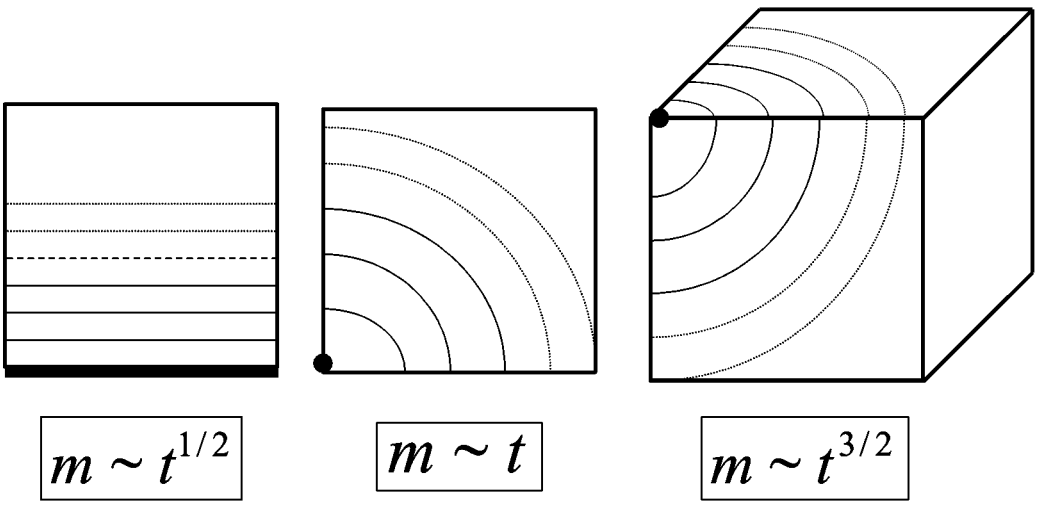

Figure 1. Possible imbibition patterns in a) 1-D geometry (plane source), b) 2-D geometry (line source), and c) 3-D geometry (point source). Lines indicate front position as a function of time.

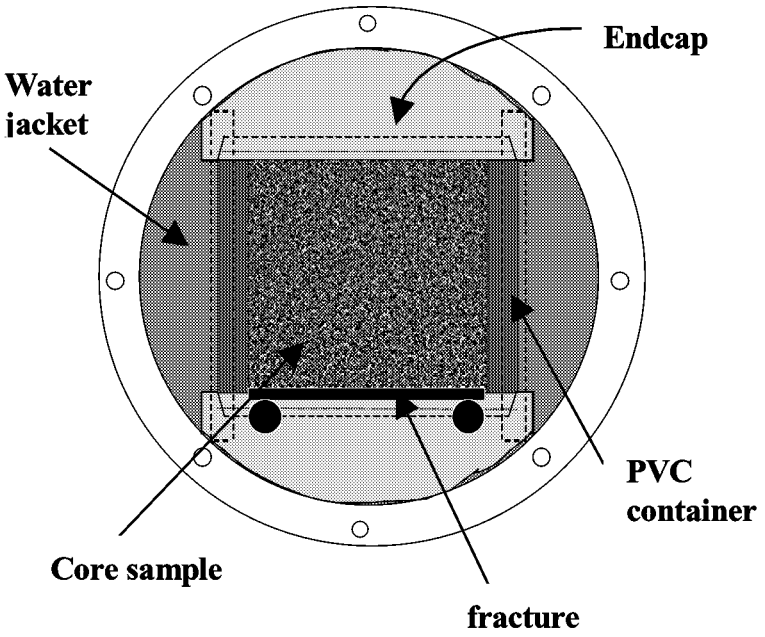

Figure 2. The core holder: Frontal view.

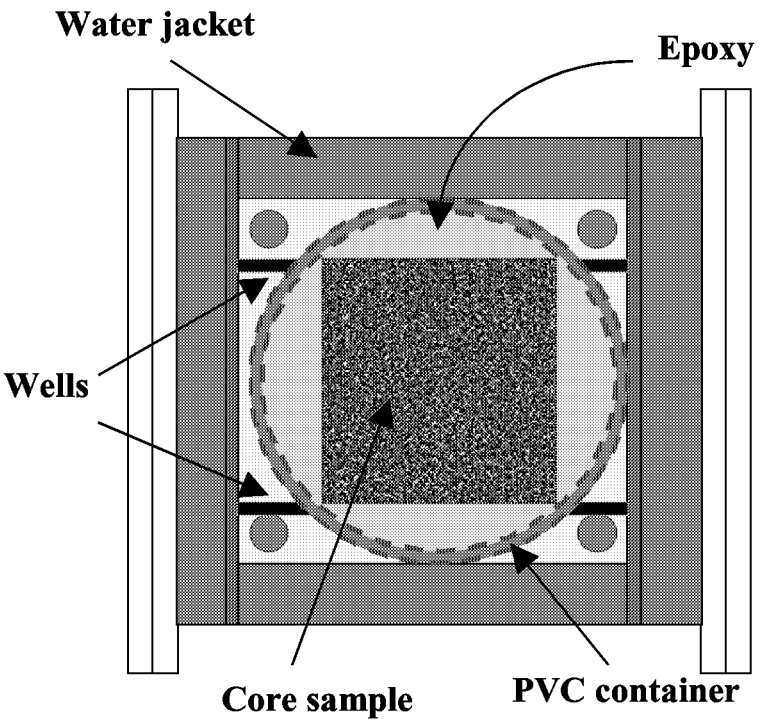

Figure 3. The core holder: Top view.

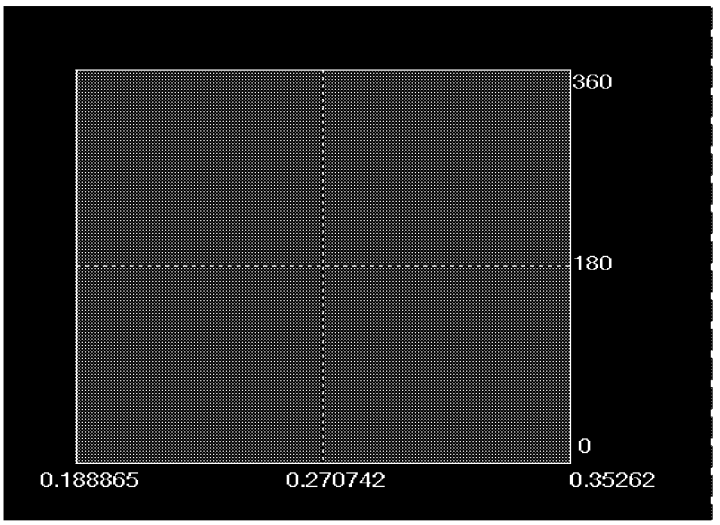

Figure 4. Frequency versus voxel porosity of Berea sandstone sample. Average porosity is 0.24 with a standard deviation of 0.01.

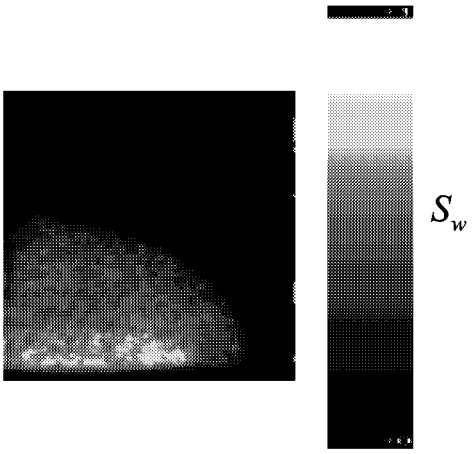

Figure 5. CT saturation image for 0.32 PV imbibed. “Filling-fracture." Aperture = 0.1 mm.

Injection rate = 1 cc/min.

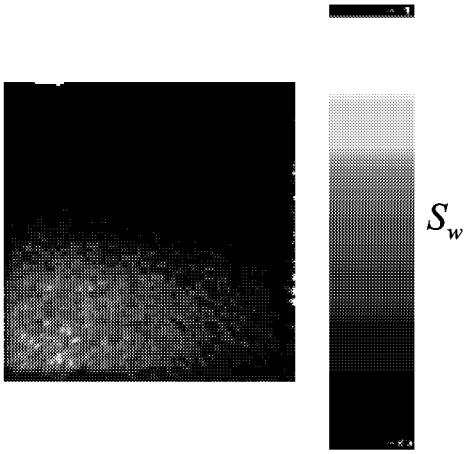

Figure 6. CT saturation image for 0.32 PV imbibed. "Instantly-filled fracture". Aperture = 0.025 mm. Injection rate = 1 cc/min.

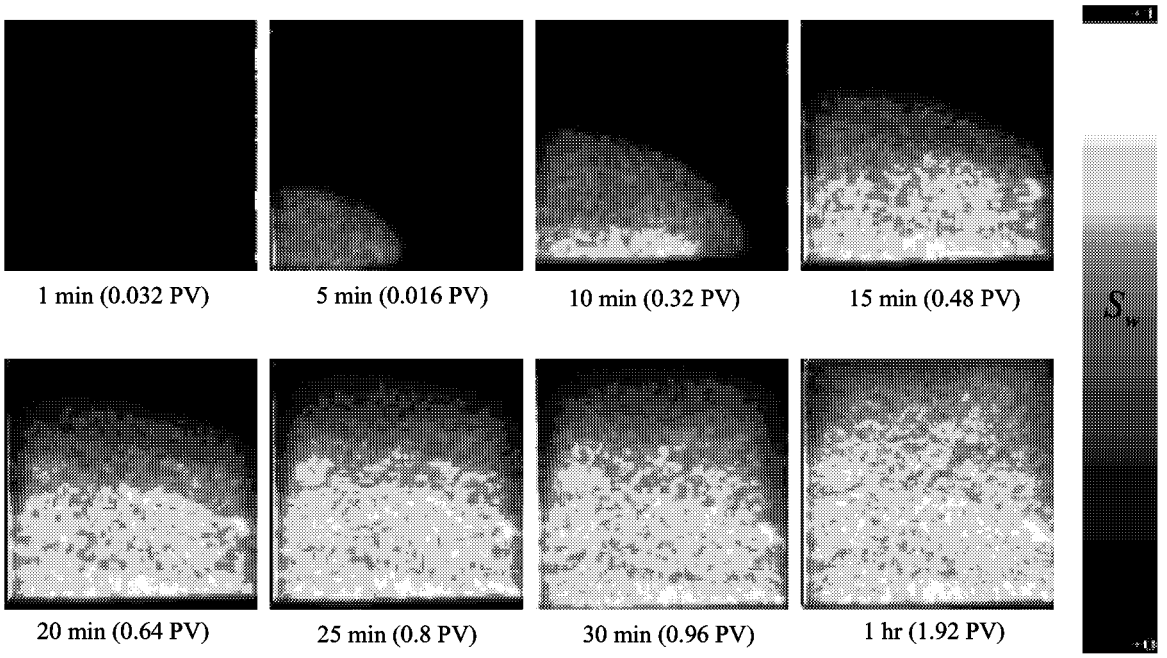

Figure 7. CT images for "filling-fracture" system for different times. Water injection at 1 cc/min in a fracture 0.1 mm thick.

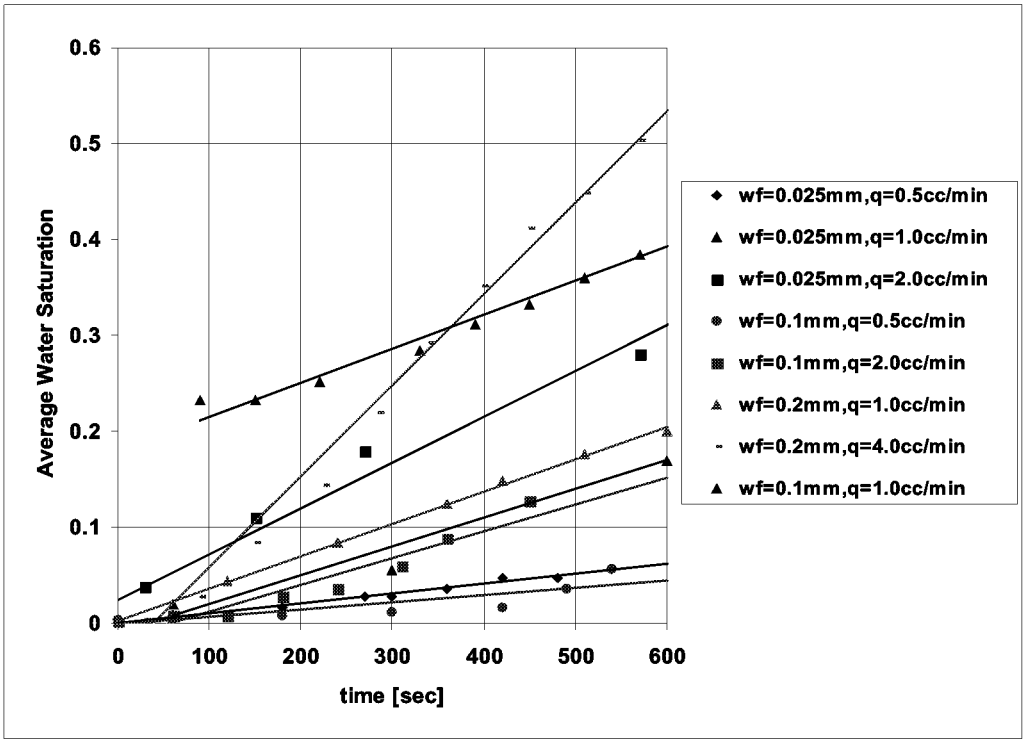

Figure 8. The average water saturation in the rock scales linearly with time. ("Filling-fracture" regime)

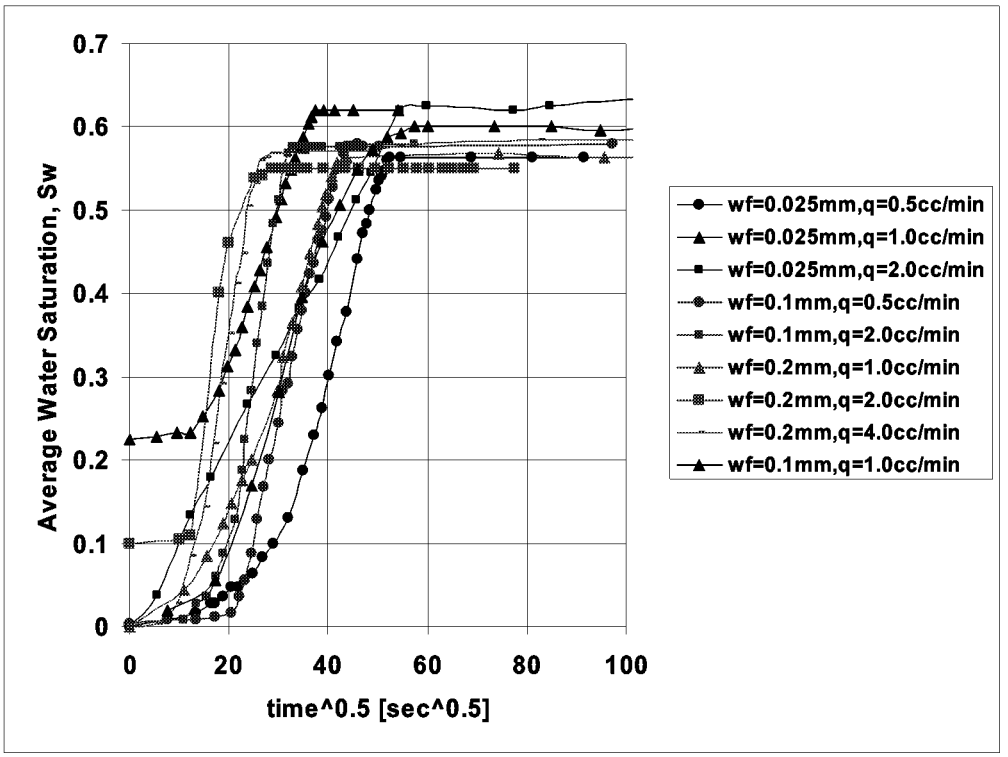

Figure 9. The average water saturation in the rock scales linearly with square root of time. ("Instantly-filled fracture" regime)

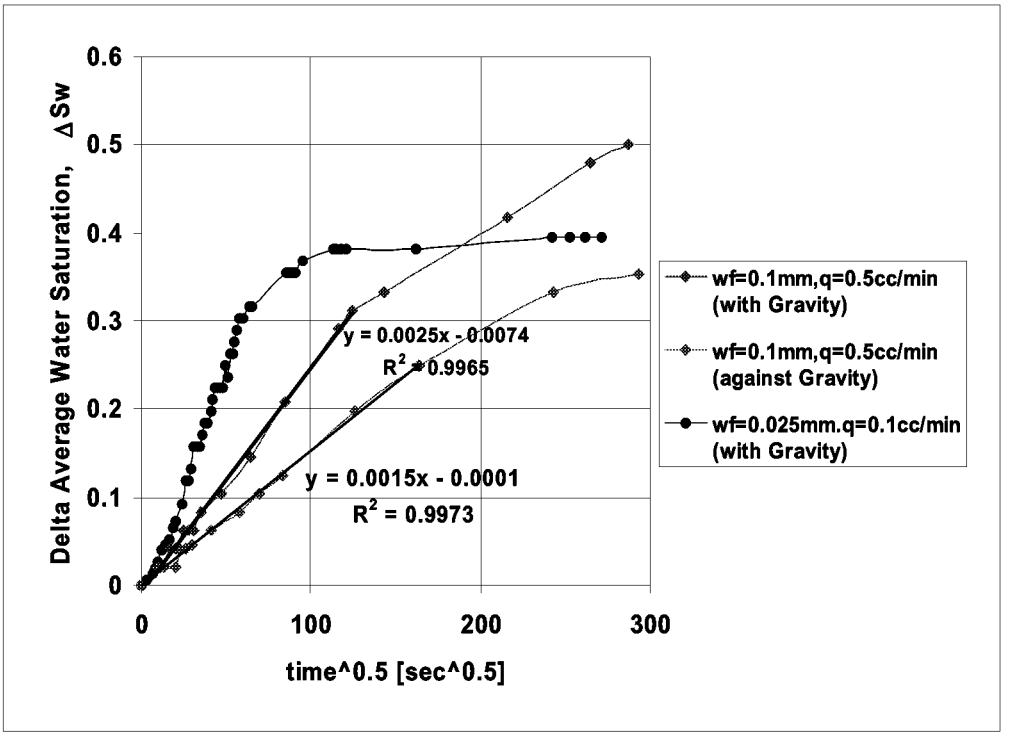

Figure 10. The average water saturation in the rock for oil-water systems.

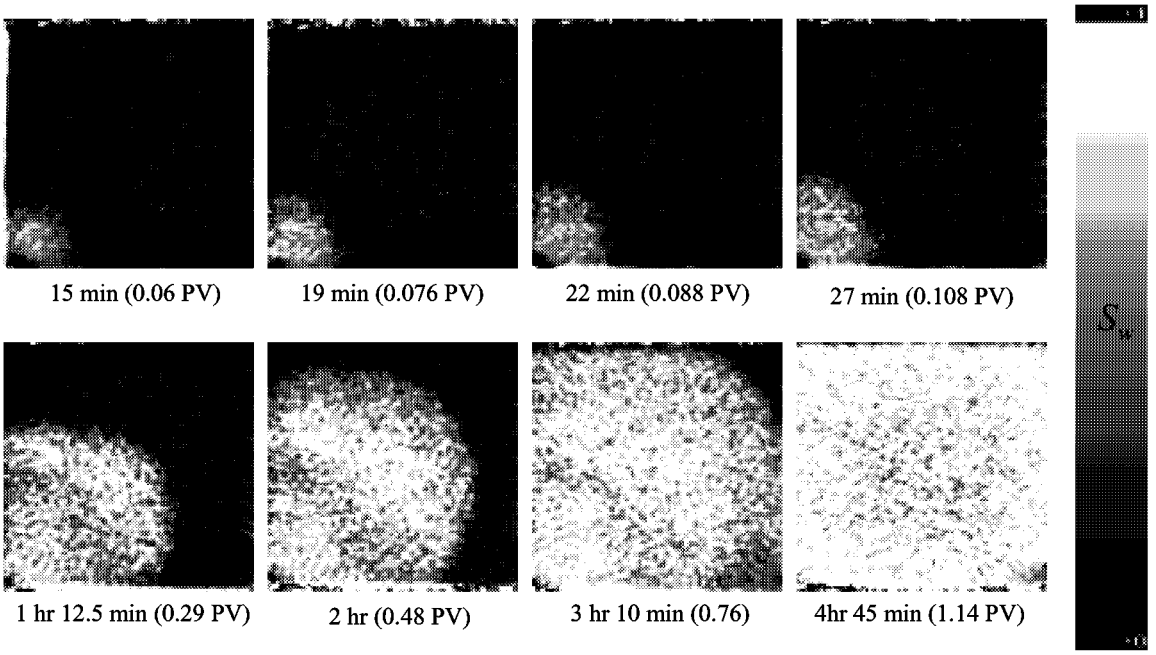

Figure 11. CT images for "filling-fracture" behavior in oil-water system for different times. Water injection at 0.1 cc/min in a fracture 0.025 mm thick.

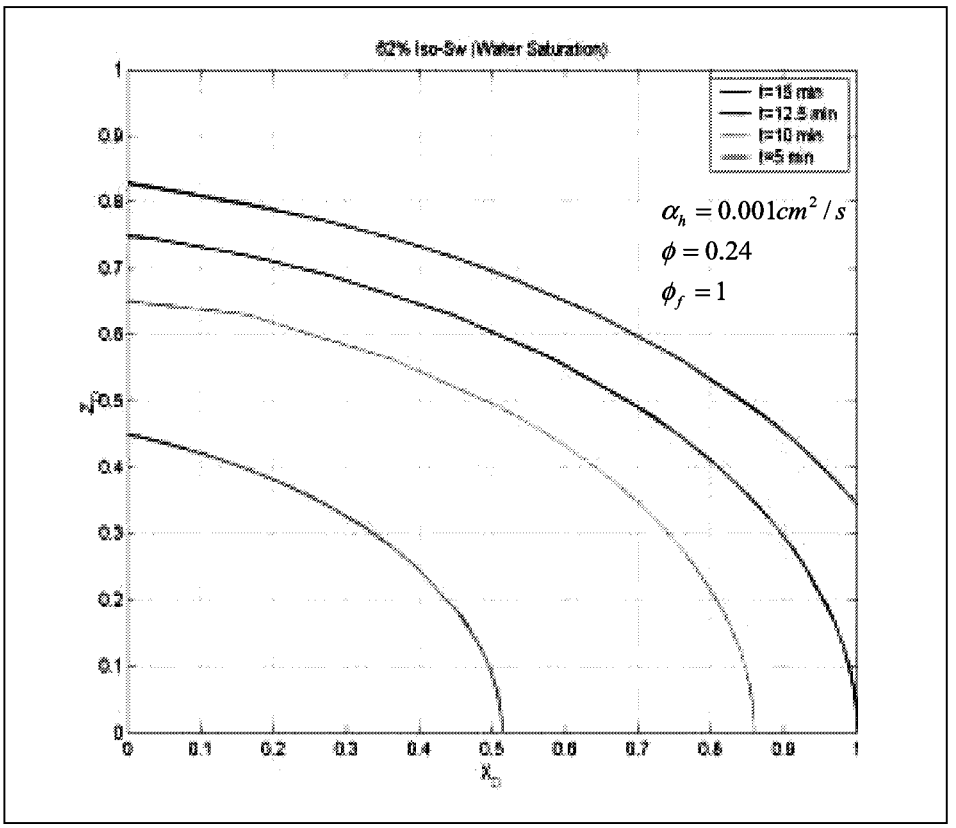

Figure 12. Water Iso-Saturation curves for different times obtained with new approach. (air-water imbibition, q = 1 cc/min, and w_f = 0.1 mm)